On the Role of Last Closed Drift Shell Dynamics in Driving Fast Losses and Van Allen Radiation Belt Extinction

L. Olifer[1] (iD), **I. R. Mann[1]** (iD), **S. K. Morley[2]** (iD), **L. G. Ozeke[1]** (iD), **and D. Choi[1]**

[1]Department of Physics, University of Alberta, Edmonton, Alberta, Canada, [2]Space Science and Applications Group, Los Alamos National Laboratory, Los Alamos, NM, USA

Abstract We present observations of very fast radiation belt loss as resolved using high time resolution electron flux data from the constellation of Global Positioning System (GPS) satellites. The time scale of these losses is revealed to be as short as $\sim$0.5–2 hr during intense magnetic storms, with some storms demonstrating almost total loss on these time scales and which we characterize as radiation belt extinction. The intense March 2013 and March 2015 storms both show such fast extinction, with a rapid recovery, while the September 2014 storm shows fast extinction but no recovery for around 2 weeks. By contrast, the moderate September 2012 storm which generated a three radiation belt morphology shows more gradual loss. We compute the last closed drift shell (LCDS) for each of these four storms and show a very strong correspondence between the LCDS and the loss patterns of trapped electrons in each storm. Most significantly, the location of the LCDS closely mirrors the high time resolution losses observed in GPS flux. The fast losses occur on a time scale shorter than the Van Allen Probes orbital period, are explained by proximity to the LCDS, and progress inward, consistent with outward transport to the LCDS by fast ultralow frequency wave radial diffusion. Expressing the location of the LCDS in L^*, and not model magnetopause standoff distance in units of R_E, clearly reveals magnetopause shadowing as the cause of the fast loss observed by the GPS satellites.

1. Introduction

Discovered in early 1958, the Van Allen radiation belts comprise highly energetic charged particles which are trapped in the Earth's magnetic field (Van Allen & Frank, 1959). Radiation belt electrons with energies from hundreds of kiloelectron volts to several megaelectron volts can be trapped on the background magnetic field. However, in response to variable solar wind forcing, the flux of these particles can change by orders of magnitude on time scales from minutes, to hours, days, months, and years (see, e.g., Mauk et al., 2013, and references therein). These radiation belt electrons also have energies that can be sufficient to penetrate spacecraft shielding and can cause damage to satellite electronics, for example, as a result of the build up of deep dielectric charging (e.g., Baker, 2002; Gubby & Evans, 2002; Wrenn, 1995). While the processes which may be responsible for the acceleration of Van Allen belt electrons to relativistic and ultrarelativistic energies have received significant attention (Albert, 2005; Horne et al., 2005; Omura et al., 2007; Shprits et al., 2008; Thorne et al., 2013), the processes which cause the loss of radiation belt electrons equally important (see, e.g., the review by Millan & Thorne, 2007, and references therein). For example, from the perspective of accurate modeling of the dynamical variations of electron flux, any fast losses that rapidly affect phase space density gradients will have a significant impact on the modeled rates of radial diffusion since these scale with the local phase space density gradient (e.g., Schulz & Lanzerotti, 1974). Similarly, in relation to the accumulation of deep dielectric charging, fast loss processes which deplete the belts can also significantly affect the expected accumulated dose and influence the deep dielectric charging resulting from the penetrating electrons.

The loss processes invoked in radiation belt depletions can be broadly grouped into two categories: loss downward into the atmosphere or loss outward across the magnetopause into interplanetary space. The former usually invokes plasma wave pitch angle scattering of electrons into the loss cone, for example, as a result of interactions with chorus waves (e.g., Shprits et al., 2007), with plasmaspheric hiss (e.g., Lee et al., 2013; Thorne et al., 1973), or with electromagnetic ion cyclotron (EMIC) waves (e.g., Kang et al., 2016; Kersten et al., 2014; Shprits et al., 2016; Summers & Thorne, 2003; Usanova et al., 2014). The latter usually

involves the inward compression of the magnetopause, and the loss of particles by magnetopause shadowing as previously closed electron drift paths become open trajectories which intersect the magnetopause (e.g., Turner et al., 2012; Xiang et al., 2017), or where such open drift paths are populated by the outward transport of electrons, for example, as a result of outward ultralow frequency (ULF) wave radial diffusion (e.g., Loto'aniu et al., 2010; Mann et al., 2016; Shprits et al., 2006).

Recently, attention has refocused on the possibility that fast ULF wave radial diffusion, coupled to fast changes in flux at the outer boundary of the belts, could act on time scales shorter than the Van Allen Probes orbital period (Mann & Ozeke, 2016). Very fast radiation belt losses were reported by Ozeke et al. (2017) in relation to the September 2014 storm, these authors highlighted that the entire belt could be globally depleted from one inbound or outbound Van Allen Probe orbit to the next. For this storm, Ozeke et al. reported global belt losses on time scales of less than 4 hr which they termed radiation belt extinction. In order to probe such fast losses, electron flux data available from the constellation of Global Positioning System (GPS) satellites have recently been used offering high time resolution monitoring on hour time scales or less (Morley et al., 2016, 2017).

Here we examine electron flux data from the Van Allen Probes together with that available from sensors on board the GPS satellite constellation to examine the time scales of storm time radiation belt loss. We compare the losses in the two intense March 2013 and March 2015 storms, as well during the extended depletion during the September 2014 storm (Ozeke et al., 2017), and in the interval of loss associated with the generation of the third radiation belt morphology observed by Baker, Kanekal, Hoxie, Henderson, et al. (2013) during the moderate September 2012 storm (see also Mann et al., 2016).

2. Data and Methodology

A summary of the solar wind, resulting geomagnetic indices, and the resulting 2.6 MeV radiation belt flux response for the March 2013, March 2015, September 2014, and September 2012 storms are shown in Figure 1. Solar wind data were taken from Operating Missions as a Node on the Internet database. Energetic particle data were taken from National Aeronautics and Space Administration's Van Allen Probes database for the Relativistic Electron-Proton Telescope (REPT) instrument (Baker, Kanekal, Hoxie, Batiste, et al., 2013). Figure 1 shows that in the first three events (March 2013, 2015, and September 2014) the radiation belt loss happened on a time scale which is too short to be fully resolved along the orbit of the Van Allen Probes mission, the orbital period being too long to provide an explicit picture of what happened. Thus, in this paper, we additionally focus on GPS satellite electron flux measurements from the Combined X-ray Dosimeter (Tuszewski et al., 2004). Combined data from 11 to 17 satellites, depending on the year, delivers high (~30 min) temporal resolution and explicitly shows the dropout patterns even in fast loss events. Note that the GPS satellites have an orbital radius of 4.2 Earth radii; therefore, the lowest McIlwain L-shell which can be observed by the constellation is $L = 4.2$. In this paper, we attempt to explain the losses seen in those four storms by magnetopause shadowing. To confirm this hypothesis, we analyze how the last closed drift shell (LCDS) which we calculate as a function of L^* compares with the observed radiation belt dropout.

It is a known problem that the calculation of the LCDS is time and resource consuming. Usually, it is done using a method described in Roederer (1970). However, to speed up calculations, a neural network was created by training it on full calculations for different events (Koller et al., 2009; Yu et al., 2012). This software is a part of the LANL* project. All calculations of any L^* parameter (Roederer, 1970) in this paper was done using TS04 Tsyganenko and Sitnov (2005) model. To be confident that the neural network returns reliable results, we compare its output and the one obtained from the full calculation for the March 2013 event. This was done by using a variant of the Roederer (1970) method to find L^* for a given second adiabatic invariant K. In this study, we use the LANLGeoMag software library (Henderson et al., 2017). It was also used in previous studies by Spence et al. (2013) and Morley et al. (2013). LCDS calculations using this approach were successfully performed by Xiang et al. (2017) for the 22–23 June 2015 event. As was shown, for example, by Ukhorskiy et al. (2011), the drift orbit of an electron can change significantly in the presence of off-equatorial magnetic field strength minima as a result of the development of Shebansky orbit (e.g., McCollough et al., 2012). The existence of Shebansky orbit effects are not accounted for the standard prescriptions by Roederer (1970) for LCDS calculations. This effect is ignored in this study.
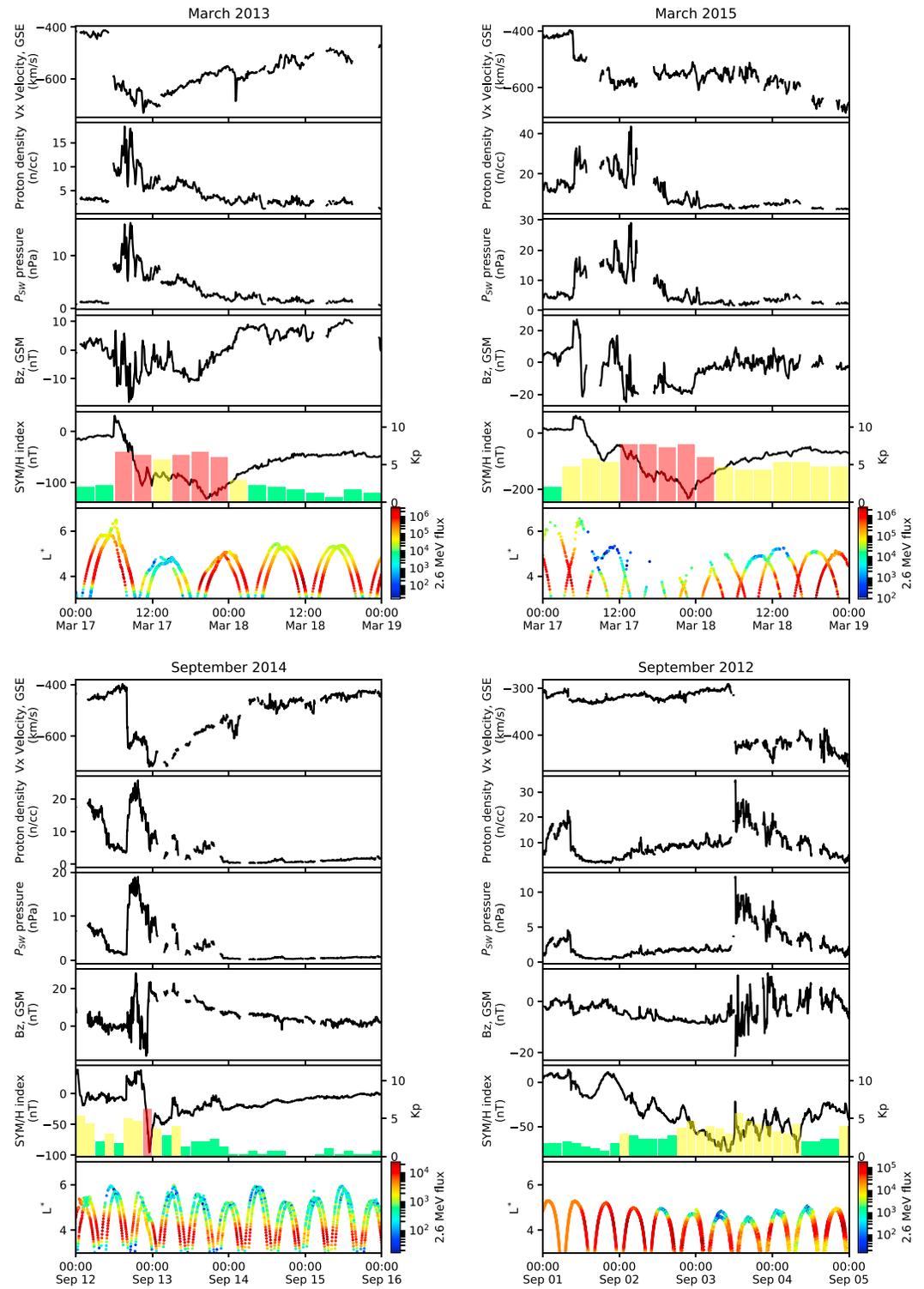
Figure 1. Summary of the solar wind, resulting geomagnetic indices, and 2.6 MeV radiation belt electron response for the March 2013, March 2015, September 2012, and September 2014 geomagnetic storms. From top to bottom for each storm: Solar wind velocity x component in GSE coordinates; proton density; solar wind dynamic pressure; z component of the interplanetary magnetic field in GSM coordinates; geomagnetic $SYM - H$ index as a line plot and Kp index as a bar plot; and 2.6 MeV electron differential flux measured by the REPT instrument on Van Allen Probes A and B as a function of L^* and time in $cm^{-2} \cdot s^{-1} \cdot sr^{-1} \cdot MeV^{-1}$.
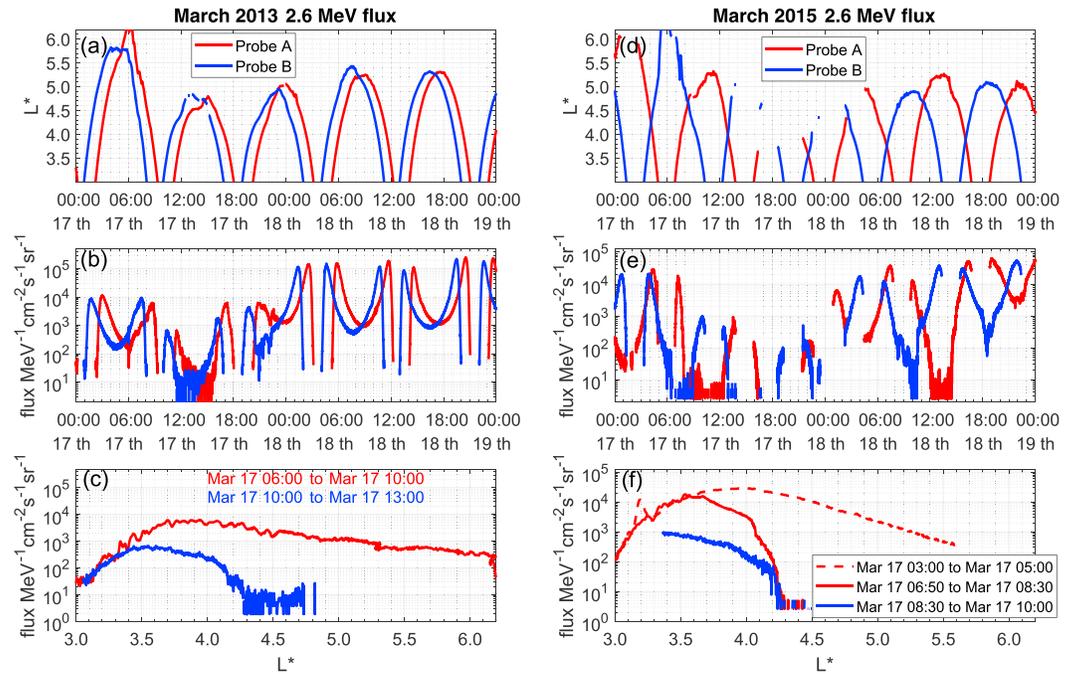
Figure 2. Summary of the Van Allen Probes A (red) and B (blue) data for the March 2013 and March 2015 storms: (top row) Van Allen Probes' L^*; (middle row) measured flux of 2.6 MeV electrons; (bottom row) L^* dependence of the flux during the fast loss. For the March 2013 storm we show the last inbound pass of Van Allen Probe A when the radiation belt is still present and the first outbound pass of Van Allen Probe B after the dropout happened. For the 2015 storm we show the last outbound pass of Probe A when the radiation belt is still present and the first inbound pass of Probe B after the dropout. With the red dashed line we show the flux measured by the inbound pass of Probe A when the first solar wind shock arrived at around 04:40 UT, but no radiation belt loss had happened yet.

3. Results

In this section, we show in situ measurements of particle fluxes from the GPS constellation of satellites as a function of L^* and time as well as detailed data from the Van Allen Probes for the March 2013, March 2015, September 2012, and September 2014 storms. Additionally, in the GPS data plots we show the LCDS as a function of L^* (left axis), calculated using LANL* neural network. The figures also show the magnetopause standoff distance in units of Earth radii (R_E), calculated using the Shue et al. (1998) model and plotted as a function of R_E on the right axis. As was mentioned in the previous section we also overlay the data for the March 2013 event with the full calculation of the L^* of the LCDS for $K = 0.11\ R_E G^{1/2}$, which corresponds to equatorial pitch angles of 50–55° in a magnetic dipole. This full LCDS calculation was done as a part of the Geospace Environment Modeling focus group "Quantitative Assessment of Radiation Belt Modeling" challenge (Brito & Morley, 2017).

3.1. March 2013 and March 2015 Storms

Figure 2 shows data from Van Allen Probes A and B for the March 2013 (left) and March 2015 (right) events wherein the top panels (a and d) show inbound and outbound passes as a function of L^* for both probes. The middle panels (b and e) show the observed flux of 2.6 MeV electrons. The bottom panels (c and f) show two Van Allen Probes passes right before and right after the fast radiation belt extinction was observed for both storms. For example, in the March 2013 event Figure 2c shows the predepletion inbound pass of Probe A and the first postdepletion outbound pass of Probe B. The differences in fluxes between those passes are at 1 order of magnitude for both storms which suggests that the main loss in both of these storms happened with a time scale much shorter than the orbital period of the Van Allen Probes. Thus, we use the GPS constellation of satellites to obtain higher time resolution. We used 12 satellites for the March 2013 event and 17 satellites for the March 2015 event, and the data are shown in Figure 3. Here we show the combined flux data for 3 MeV electrons as a function of L^* (left axis), the LCDS as a function of L^* calculated using the LANL* neural network with a red lines, and the full LCDS calculation for the March 2013 event with a blue line. As described above
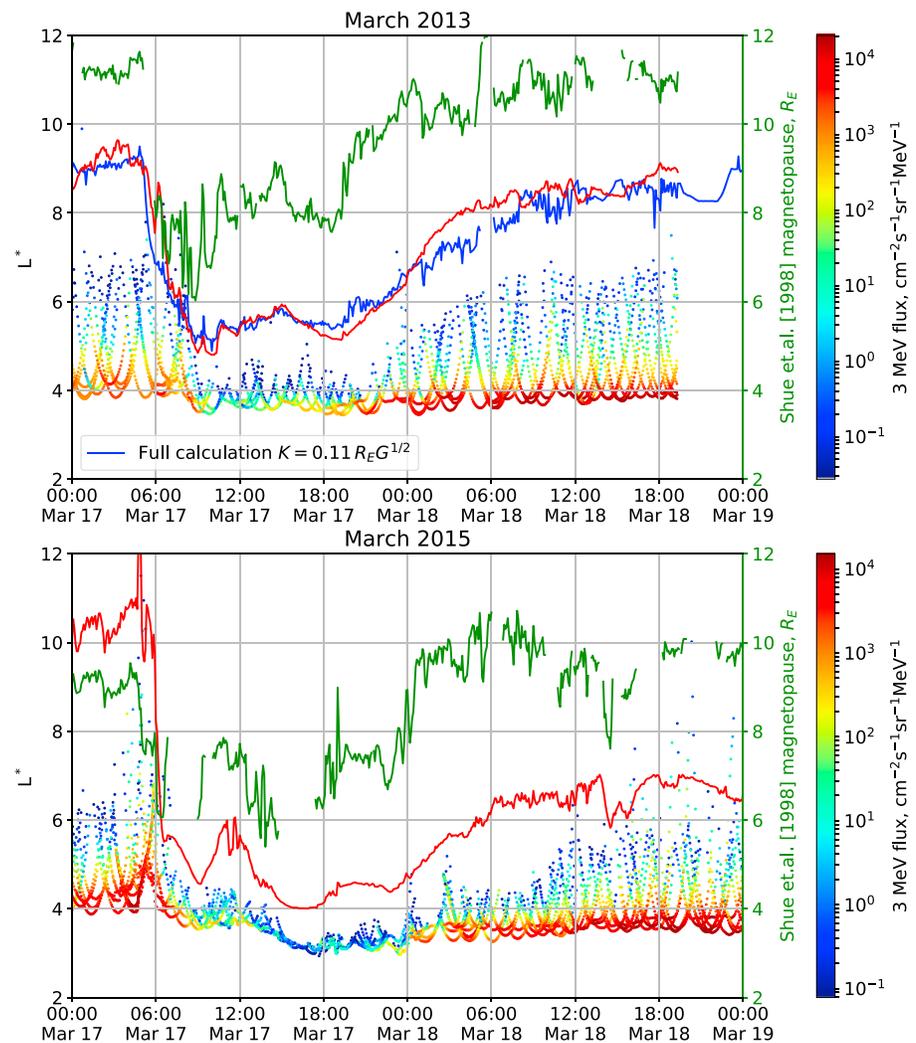
Figure 3. The 3 MeV electron flux from the Global Positioning System constellation as a function of $L*$ (left axis) for the March 2013 and March 2015 storms. Last closed drift shell $L*$, calculated using LANL* neural network, is shown with a red line. The magnetopause standoff distance in units of Earth radii, calculated using Shue et al. (1998) model, is shown with a green line and should be read from the right-hand axis. For the 2013 event we also show the full calculation for the $L*$ of the last closed drift shell with a blue line (see text for details).

the magnetopause position in units of Earth radii R_E calculated using Shue et al. (1998) model is also shown with a green line using the right-hand axis.

Apart from the clear correspondence between the LCDS and the flux data in Figure 3, we also note how well the neural network reproduces results from the full simulation for a moderately low second adiabatic invariant, K, for the March 2013 event (the top panel of Figure 3). We also note that the LCDS derived from the full calculations for different values of K is qualitatively similar and only shows a small offset as a function of K. Based on this result, we are confident that the LANL* neural network LCDS calculation approach can give quite accurate results. For numerical efficiency, for the subsequent three storms we hence calculate the LCDS with the LANL* neural network approach. Note also that for the period around 5–6 UT on 18 March 2013, there is a strong anomaly in the full LCDS calculation, and this interval is not plotted in Figure 3.

Figure 3 shows a remarkable high time resolution coherence between the location of the LCDS, its proximity to the Van Allen Belt, and the observed fast loss as characterized in GPS electron flux data. The strong correlation between measured flux and LCDS is present for both of these storms. They were so powerful that the LCDS dropped down to $L* \sim 5$ and $L* \sim 4$ in 2013 and 2015, respectively, for a relatively long time of ~6 hr. For the March 2013 storm, the LCDS gradually moves inward following the storm commencement and significant

belt losses are observed early in the main phase before the minimum in $SYM − H$. Losses are seen clearly in Van Allen Probe data (Figure 2) at L^*= 4.5 between around 08 UT and 12 UT, and at L^*= 4 between around 08:30 UT and 11 UT. The GPS data (Figure 3, top panel) reveal the spatiotemporal characteristics of this loss in much greater detail, with rapid loss occurring around 08–09 UT and with losses moving inward deeper into the belt in concert with the inward motion of the LCDS from $L^*\sim$ 6 to $L^*\sim$ 5. Van Allen Probe data suggest that the losses have reached inside GPS orbit to at least $L^*\lesssim$ 3.5 by ∼10:20 UT. For March 2013 there remains a separation between the LCDS and the L^* where the loss is observed since the LCDS does not drop below $L^*\sim$ 5. However, in the presence of steep gradients in phase space density and strong storm main phase ULF wave power (Dimitrakoudis et al., 2015; Murphy et al., 2015) the time scales in the modeling of Mann and Ozeke (2016) suggest that outward radial diffusion to the LCDS could be sufficient to explain the observed rapid losses and radiation belt extinction.

Arguably, the March 2015 event shows even faster loss. As described by Baker et al. (2016) and as can be seen from Figure 1, a solar wind shock arrives around 04:40 UT and the magnetopause position moves in by ≈2 L. This shock arrival was discussed in detail by Baker et al. (2016, their Figure 7) who emphasized the generation of drift echoes following the shock impact. However, the GPS data do not show any signs of loss until after 06:00 UT. This is the time that the interplanetary magnetic field (IMF) turns southward, and the LCDS moves inward with the loss starts immediately after (Figure 1 top right plot). For the March 2013 event, which was discussed by Baker et al. (2014), the IMF turns southward almost immediately at storm onset which causes the LCDS and the magnetopause to move inward at the same time. This implies that the governing factor of the loss in both of these events is the location of the LCDS. Note, however, that it is crucial to take the LCDS location into consideration as a function of L^* rather than regarding the Shue et al. (1998) magnetopause location in units of Earth radii as being equivalent to the LCDS position in L^*.

Additionally to GPS flux data for 3 MeV electrons, we present data for a wider range of GPS energies in the supporting information for this paper. Figure S1 shows that similar dropouts also happened for different energy populations, and all of them follow the same trend as the LCDS. The fact that a wide range of energies show similar behavior is consistent with the response expected for magnetopause shadowing but is most likely inconsistent with the hypothesis that plasma wave-particle scattering into the atmosphere was the dominant loss process. The very fast, $\lesssim$ hour time scale, losses of at least an order of magnitude in flux revealed by the GPS satellites suggest that these losses might be described in terms of radiation belt extinction, consistent with the characteristics of the very fast losses reported by Ozeke et al. (2017) for the September 2014 storm.

3.2. September 2014 and September 2012 Storms

Similar to the previous subsections we show the data from Van Allen Probes A and B for the September 2014 and September 2012 events in Figure 4. Figure 4c shows the last predepletion outbound pass of Probe A and the first postdepletion inbound pass of Probe B. As discussed by Ozeke et al. (2017) and shown in Figure 4 here, the loss in the September 2014 event (Figures 4a–4c) can also be characterized in terms of radiation belt extinction. In contrast, losses in the September 2012 event (Figures 4d–4f) are more gradual.

GPS data for the September 2014 and September 2012 storms are shown in Figure 5 in the same format as Figure 3. Note that here we analyze events not in chronological order since the loss characteristics during the September 2014 event are closer to those also seen for the March 2013 and March 2015 events; in all three cases the depletion happened very fast ($\lesssim$0.5–2 hr). In contrast, the September 2012 event has a more gradual loss. For the September 2014 event, the top panel of Figure 5 shows that despite the sudden inward motion of the magnetopause at 16:00 UT on 12 September 2014, the loss does not start until the IMF turns southward at 20:15 UT and when the LCDS rapidly moves inward to $L^*\approx$ 5. Even this short inward excursion of the LCDS is sufficient to cause the fast losses and belt extinction.

For the September 2012 event (bottom panel of Figure 5) the IMF turns southward at the beginning of the storm but only gradually increases in its magnitude over the next 48 hr. The LCDS gradually moves inward during this interval to reach $L^*\approx$ 6. Significantly, the magnetopause remains at a standoff distance of $\gtrsim$10 Earth radii throughout this interval until the shock arrival at around 12 UT on 3 September. Note that this event, although characterized by the generation of a third radiation belt, was only a moderate storm with $SYM − H$ only reaching a minimum of −77 nT. Figure 4 shows that the Van Allen Probes reveal a period of rather gradual loss in September 2012, in advance of the arrival of the interplanetary shock. This is consistent with the analysis by Mann et al. (2016) who asserted that outward ULF wave radial diffusion was responsible for the losses during this storm and which began in advance of the shock arrival. Interestingly, as shown
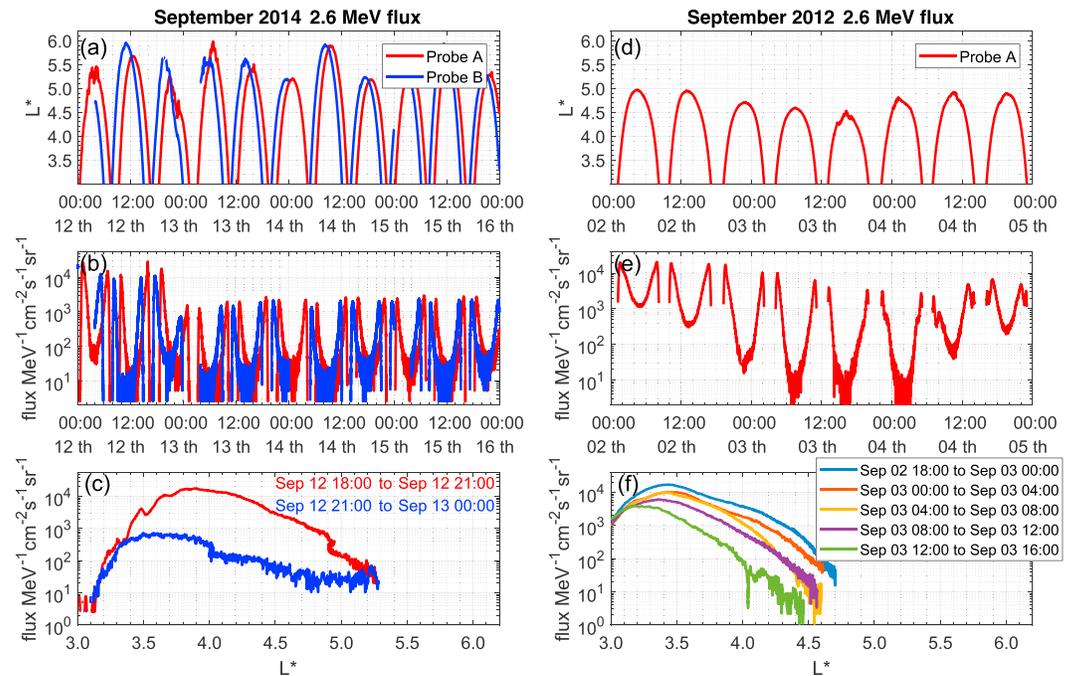
Figure 4. Summary of the Van Allen Probes A (red) and B (blue) data for the September 2014 and 2012 storms: (top row) Van Allen Probes' L*; (middle row) measured flux of 2.6 MeV electrons; (bottom row) L* dependence of the flux during the fast loss. For the September 2014 storm we show the last outbound pass of Probe A when the radiation belt is still present and the first inbound pass of Probe B after the dropout. For 2012 storm we show gradual loss with different colors, which happened through multiple orbits of Van Allen Probe A.

in Figure 5 (bottom panel), at GPS altitudes the shock does not seem to be associated with additional fast losses, although as the LCDS moves in further the fluxes at GPS gradually are further reduced in concert with the proximity of the LCDS.

Overall, Figure 5 emphasizes the importance of the proximity of the calculated LCDS as a function of L* for assessing radiation belt losses, as opposed to merely regarding Shue et al. (1998) magnetopause location in units of R_E as an approximation for the L* of the LCDS. Consistent with the analysis of the LCDS in Alves et al. (2016), the September 2014 storm is characterized by fast outward losses through the LCDS. During this event, the LCDS remains at L* ≈ 6 for a couple of hours, presumably low enough in L* for fast outward ULF wave transport to create the observed extinction. This contrasts with the September 2012 event where, consistent with the calculations of Mann et al. (2016), a more distant LCDS appears to lead to a more gradual rate of loss for the belts. For these September storm events, we also present data for additional GPS energy channels in the supporting information to this paper (Figure S2). Data from this wider range of energy channels again support the conclusion that outward transport to the LCDS was responsible for the observed losses.

3.3. Loss Time Scales

It is also relevant to analyze the time dependence of the mean GPS flux as a function of McIlwain L-shell to study the morphology of the dropouts from a different perspective. These data are shown in Figure 6 for the March 2013 and 2015 events, and in Figure 7 for September 2014 and 2012. Each of the plots shows the average flux measured by the GPS satellites, which are present in the specified L-shell bins. Figure 6 shows that for both the March 2013 and March 2015 events the dropouts happened first at high L-shell and then later at lower L-shell. Note that on 17 March 2015, following the dropout, the data on the higher L-shells are close to the noise floor and not shown. Figure 6 shows the same picture for both March storms with depletion on higher L-shells happening earlier than on the lower L-shells. Very significantly this indicates an inward propagation of loss consistent with magnetopause shadowing.

What is also very clearly seen in Figures 6 and 7, at least for the March 2013, March 2015, and September 2014 events, is that the time scale of the loss is very short, only ~0.5–2 hr, depending on the storm and L-shell bin. In all of these cases, the fastest losses occurred at the highest L-shells, while more gradual losses happened
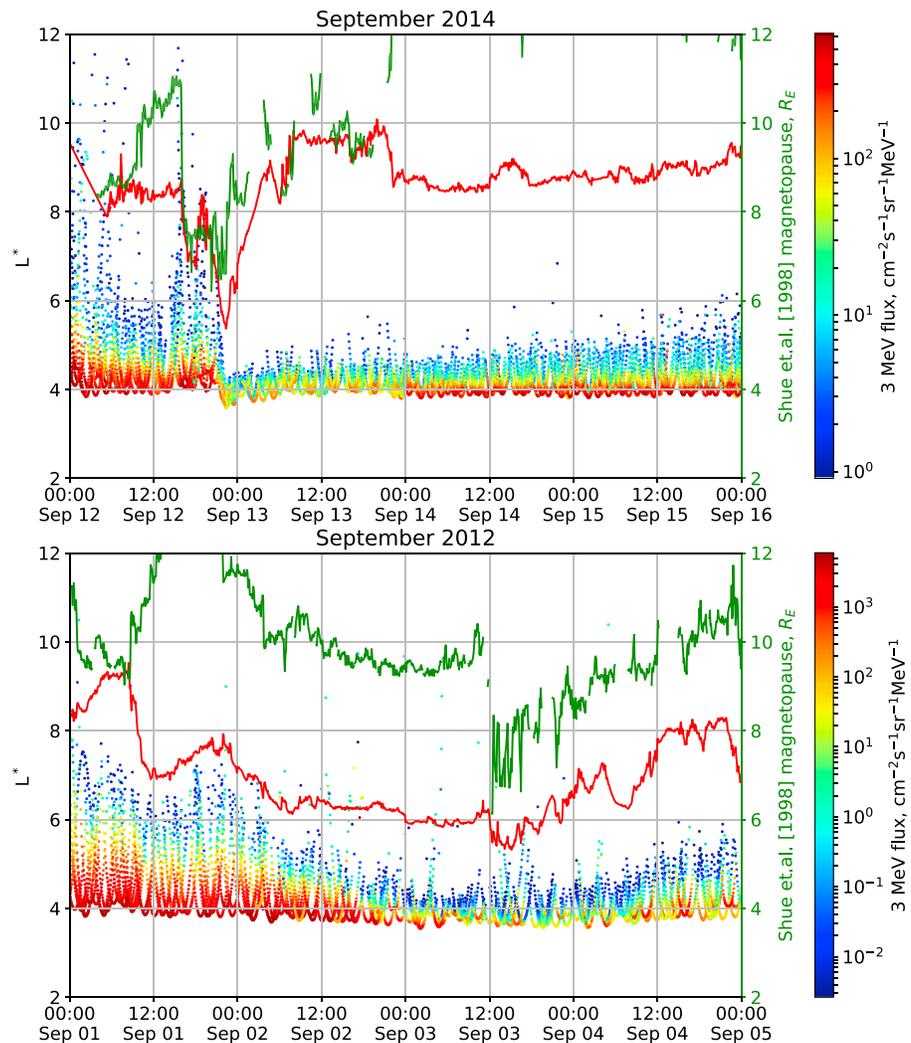
Figure 5. The 3 MeV electron flux from the Global Positioning System satellite constellation as a function of L^* (left axis) for the September 2012 and September 2014 storms. Last closed drift shell L^*, calculated using LANL* neural network, is shown with a red line. The magnetopause standoff distance in units of Earth radii, calculated using Shue et al. (1998) model, is shown with a green line and should be read from the right-hand axis. Note that for the September 2014 event the Shue et al. (1998) model gives a magnetopause position >12 L for an extended period of time.

at lower L-shells but still within a short ∼2 hr time scale. The same overall pattern is also seen for the September 2012 storm, again with faster losses at higher L-shells and overall inward propagation of losses—consistent with magnetopause shadowing as proposed by Mann et al. (2016)—just on relatively slower time scales.

The September 2012 storm was characterized by losses at higher L-shells, which left the remnant belt at the inner edge of the outer zone. Following subsequent flux recovery on higher L-shells, this resulted in a third belt morphology with a flux gap between the remnant belt and the newly recovered outer belt (Baker, Kanekal, Hoxie, Henderson, et al., 2013). Shprits et al. (2013) introduced localized EMIC wave losses in the gap region into their modeling in order to reproduce the observed third belt morphology. More recently, Mann et al. (2016) argued that the remnant belt could be produced by outward ULF wave radial diffusion to the magnetopause and that the third belt morphology did not require the action of EMIC waves. Shprits et al. (2018) argue that the conclusions of Mann et al. (2016) are incorrect and reiterate that in their view EMIC waves are necessary to create the third belt. In their reply to the Shprits et al. (2018) comment, Mann et al. (2018) present phase space density profiles which decrease with L^* during the loss period consistent with their earlier hypothesis that magnetopause shadowing explains the creation of the third belt. The GPS and LCDS data
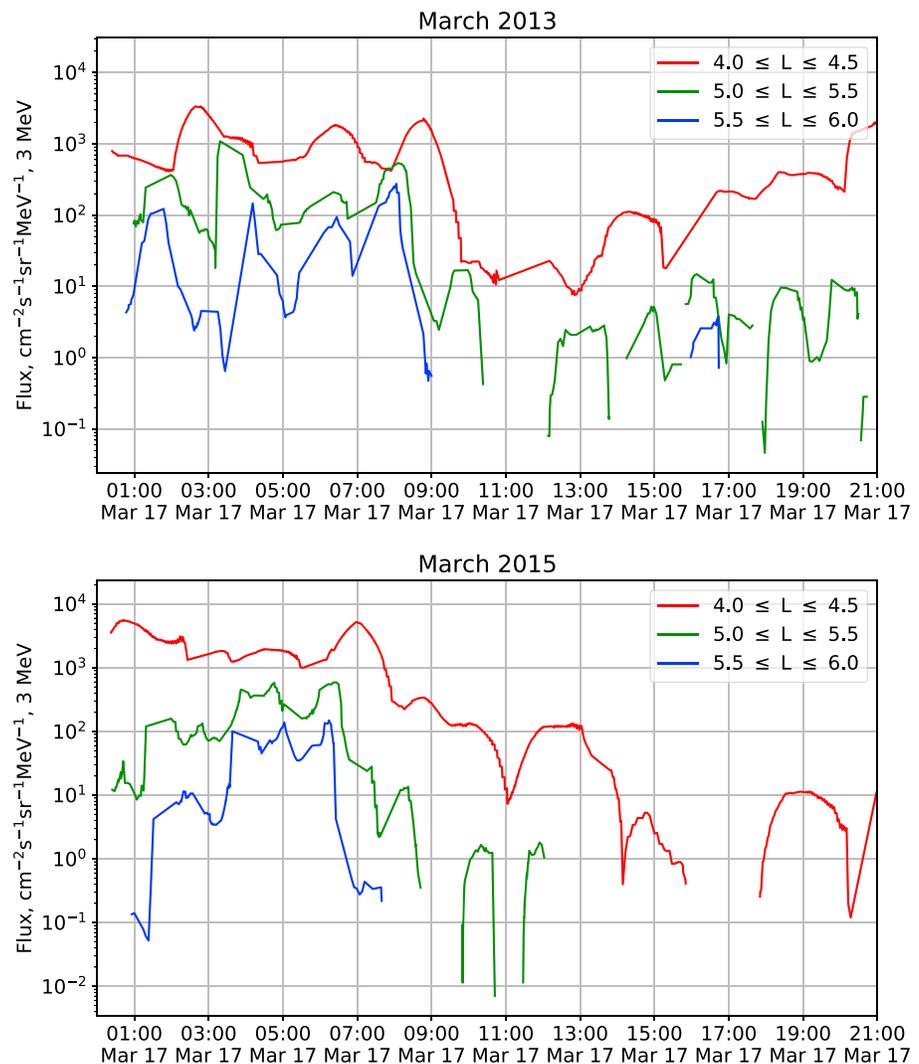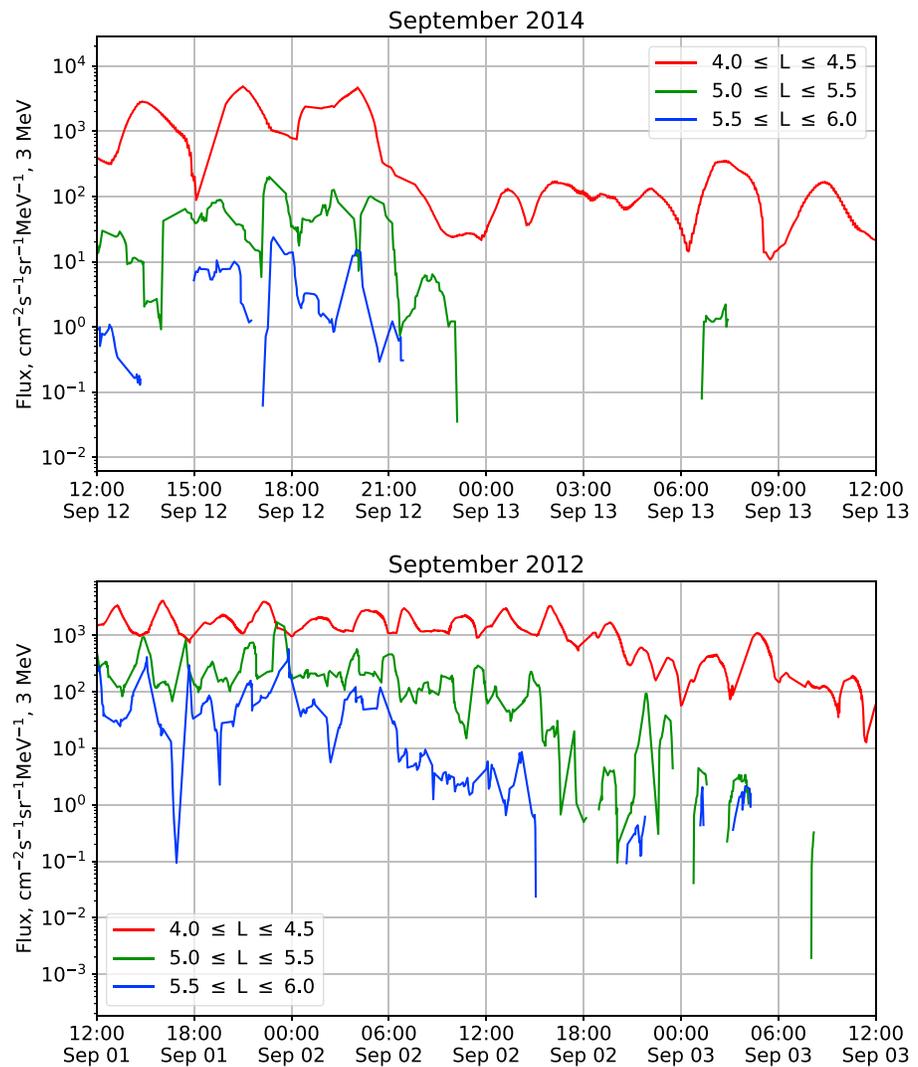
Figure 6. Time dependence of mean 3 MeV electron flux observed from the Global Positioning System satellite constellation binned in three L-shell ranges for the March 2013 and March 2015 storms.

in Figure 5 appear to be consistent with the conclusion of Mann et al. (2016, 2018) that gradual outward ULF wave transport and magnetopause shadowing losses played a large role in creating the third radiation belt morphology.

4. Discussion and Conclusions

It is worthwhile to compare the results presented here to the results presented by Morley et al. (2010). These authors compared the GPS electron flux as a function of dipole L observed in 61 sudden impulse events and superposed them with Shue et al. (1998) magnetopause location. The Morley et al. study hence clearly suggested a substantial role for solar wind compressions, a result which has also been reported in subsequent studies. However, for the sudden impulse events in the Morley et al. superposition, the magnetopause remained ~2–3 L-shells away from the location of the observed GPS losses. However, as we show here, when the location of the LCDS is calculated as a function of L^* it lies much closer to the radiation belt where the losses are observed. As discussed by Mann et al. (2016), the remaining separation between the LCDS and the radiation belt can also be bridged by ULF wave outward radial diffusion. Our results imply that fast outward diffusion to a proximal LCDS can not only result in fast losses but under the appropriate conditions during intense storms, that such losses can create radiation belt extinctions and which can have a global effect on very fast time scales. As we showed here, such loss time scales are much shorter than the orbital periods

Figure 7. Time dependence of mean 3 MeV electron flux observed from the Global Positioning System satellite constellation binned in three L-shell ranges for the September 2014 and September 2012 storms. Note that only 24 hr of data is shown for September 2014, while 48 hr is shown for September 2012.

of the Van Allen Probes. As we further demonstrated here, combining electron flux data for the constellation of GPS satellites allows such very fast radiation belt losses to be resolved, at least at the altitudes and L-shell ranges covered by the GPS satellite constellation.

Overall, Morley et al. (2010) showed that there is a correlation between the radiation belt loss patterns in a geomagnetic storm and the dynamics of the magnetopause (classically calculated using the Shue et al., 1998, model). Similar patterns are present in some of the events from this paper. However, a much stronger correlation exists between the loss trends and the LCDS when calculated as a function of $L*$. This LCDS correlation holds even for the rapid radiation belt extinction events of March 2015 and September 2014, and for these events, the inward motion of the magnetopause standoff is inconsistent with the timing of the actual dropout. This implies that the crucial factor governing the loss in these events is the location of the LCDS. As the outer boundary in those events, losses at the LCDS will produce steep gradients in particle phase density in much closer proximity to the heart of radiation belt than implied by assuming it occurs on L-shells equal to the standoff distance in the Shue et al. (1998) magnetopause model. In our view in order to accurately model ULF wave outward transport, which is mostly governed by steep gradients in phase space density, the calculated $L*$ location of the LCDS is likely the key.

Studies of the temporal evolution of electron fluxes on different L-shells (Figures 6 and 7), as well as across a wide range of energies (see supporting information), reinforce our conclusion that transport to the LCDS and related magnetopause shadowing were the primary cause of the loss in the four storms studied here. In particular, the fact that the loss moves inward and happens first on high L-shells and later on lower L-shells is consistent with outward ULF wave transport to an outer boundary determined in our case by calculation of the LCDS. Additionally, the observed loss patterns are the same for different energies from 1 to 5 MeV (see supporting information for this paper), and all of them are strongly correlated with the LCDS. Our analysis was done using high-resolution data from all available GPS satellites. This allows us to study electron flux dynamics with ≈ 30 min temporal and ≈ 0.25 Earth radii spatial resolution, as opposed to the ≈ 9 hr orbital period of the Van Allen Probes.

In this study, we used the LANL* neural network to perform the calculation of the LCDS. This approach has a tremendous advantage over the full calculation method in terms of the required computational resources. However, the neural network itself does not have any knowledge of the governing physics. Nevertheless, it was shown that the LCDS calculated using the LANL* neural network agreed well with the full LCDS calculation, at least for the March 2013 storm where we completed a validation. All of the above implies that when assessing magnetopause shadowing losses in the Van Allen radiation belts analyzing the LCDS and working in $L*$ space is more reasonable than regarding a classical Shue et al. (1998) model of magnetopause standoff distance in terms of Earth radii as the L-shell where shadowing losses will occur.

References

Albert, J. M. (2005). Evaluation of quasi-linear diffusion coefficients for whistler mode waves in a plasma with arbitrary density ratio. *Journal of Geophysical Research*, 110, A03218. https://doi.org/10.1029/2004JA010844

Alves, L. R., Da Silva, L. A., Souza, V. M., Sibeck, D. G., Jauer, P. R., Vieira, L. E. A., et al. (2016). Outer radiation belt dropout dynamics following the arrival of two interplanetary coronal mass ejections. *Geophysical Research Letters*, 43, 978–987. https://doi.org/10.1002/2015GL067066

Baker, D. N. (2002). How to cope with space weather. *Science*, 297(5586), 1486–1487. https://doi.org/10.1126/science.1074956

Baker, D. N., Jaynes, A. N., Kanekal, S. G., Foster, J. C., Erickson, P. J., Fennell, J. F., et al. (2016). Highly relativistic radiation belt electron acceleration, transport, and loss: Large solar storm events of March and June 2015. *Journal of Geophysical Research: Space Physics*, 121, 6647–6660. https://doi.org/10.1002/2016JA022502

Baker, D. N., Jaynes, A. N., Li, X., Henderson, M. G., Kanekal, S. G., Reeves, G. D., et al. (2014). Gradual diffusion and punctuated phase space density enhancements of highly relativistic electrons: Van Allen Probes observations. *Geophysical Research Letters*, 41, 1351–1358. https://doi.org/10.1002/2013GL058942

Baker, D. N., Kanekal, S. G., Hoxie, V. C., Batiste, S., Bolton, M., Li, X., et al. (2013). The Relativistic Electron-Proton Telescope (REPT) Instrument on board the Radiation Belt Storm Probes (RBSP) Spacecraft: Characterization of Earth's radiation belt high-energy particle populations. *Space Science Reviews*, 179(1), 337–381. https://doi.org/10.1007/s11214-012-9950-9

Baker, D. N., Kanekal, S. G., Hoxie, V. C., Henderson, M. G., Li, X., Spence, H. E., et al. (2013). A long-lived relativistic electron storage ring embedded in Earth outer Van Allen Belt. *Science*, 340(6129), 186–190. https://doi.org/10.1126/science.1233518

Brito, T. V., & Morley, S. K. (2017). Improving empirical magnetic field models by fitting to in situ data using an optimized parameter approach. *Space Weather*, 15, 1628–1648. https://doi.org/10.1002/2017SW001702

Dimitrakoudis, S., Mann, I. R., Balasis, G., Papadimitriou, C., Anastasiadis, A., & Daglis, I. A. (2015). Accurately specifying storm-time ULF wave radial diffusion in the radiation belts. *Geophysical Research Letters*, 42, 5711–5718. https://doi.org/10.1002/2015GL064707

Gubby, R., & Evans, J. (2002). Space environment effects and satellite design. *Journal of Atmospheric and Solar-Terrestrial Physics*, 64(16), 1723–1733. https://doi.org/10.1016/S1364-6826(02)00122-0, space Weather Effects on Technological Systems.

Henderson, M., Morley, S., Niehof, J., & Larsen, B. (2017). drsteve/LANLGeoMag: LANLGeoMag v.1.5.15-alpha. https://doi.org/10.5281/zenodo.1133782

Horne, R. B., Thorne, R. M., Glauert, S. A., Albert, J. M., Meredith, N. P., & Anderson, R. R. (2005). Timescale for radiation belt electron acceleration by whistler mode chorus waves. *Journal of Geophysical Research*, 110, A03225. https://doi.org/10.1029/2004JA010811

Kang, S.-B., Fok, M.-C., Glocer, A., Min, K.-W., Choi, C.-R., Choi, E., & Hwang, J. (2016). Simulation of a rapid dropout event for highly relativistic electrons with the RBE model. *Journal of Geophysical Research: Space Physics*, 121, 4092–4102. https://doi.org/10.1002/2015JA021966

Kersten, T., Horne, R. B., Glauert, S. A., Meredith, N. P., Fraser, B. J., & Grew, R. S. (2014). Electron losses from the radiation belts caused by EMIC waves. *Journal of Geophysical Research: Space Physics*, 119, 8820–8837. https://doi.org/10.1002/2014JA020366

Koller, J., Reeves, G. D., & Friedel, R. H. W. (2009). LANL* V1.0: A radiation belt drift shell model suitable for real-time and reanalysis applications. *Geoscientific Model Development*, 2(2), 113–122. https://doi.org/10.5194/gmd-2-113-2009

Lee, J., Min, K., & Kim, K. (2013). Characteristic dimension of electromagnetic ion cyclotron wave activity in the magnetosphere. *Journal of Geophysical Research: Space Physics*, 118, 1651–1658. https://doi.org/10.1002/jgra.50242

Loto'aniu, T. M., Singer, H. J., Waters, C. L., Angelopoulos, V., Mann, I. R., Elkington, S. R., & Bonnell, J. W. (2010). Relativistic electron loss due to ultralow frequency waves and enhanced outward radial diffusion. *Journal of Geophysical Research*, 115, a12245. https://doi.org/10.1029/2010JA015755

Mann, I. R., & Ozeke, L. G. (2016). How quickly, how deeply, and how strongly can dynamical outer boundary conditions impact Van Allen radiation belt morphology?. *Journal of Geophysical Research: Space Physics*, 121, 5553–5558. https://doi.org/10.1002/2016JA022647

Mann, I. R., Ozeke, L. G., Morley, S. K., Murphy, K. R., Claudepierre, S. G., Turner, D. L., et al. (2018). Reply to 'The dynamics of Van Allen belts revisited'. *Nature Physics*, 14, 103–104. https://doi.org/10.1038/nphys4351

Mann, I. R., Ozeke, L. G., Murphy, K. R., Claudepierre, S. G., Turner, D. L., Baker, D. N., et al. (2016). Explaining the dynamics of the ultra-relativistic third Van Allen radiation belt. *Nature Physics*, 12, 978–983. https://doi.org/10.1038/nphys3799

Mauk, B. H., Fox, N. J., Kanekal, S. G., Kessel, R. L., Sibeck, D. G., & Ukhorskiy, A. (2013). Science objectives and rationale for the Radiation Belt Storm Probes Mission. *Space Science Reviews*, 179(1), 3–27. https://doi.org/10.1007/s11214-012-9908-y

McCollough, J. P., Elkington, S. R., & Baker, D. N. (2012). The role of Shabansky orbits in compression-related electromagnetic ion cyclotron wave growth. *Journal of Geophysical Research*, *117*, A01208. https://doi.org/10.1029/2011JA016948

Millan, R., & Thorne, R. (2007). Review of radiation belt relativistic electron losses. *Journal of Atmospheric and Solar-Terrestrial Physics*, *69*(3), 362–377. https://doi.org/10.1016/j.jastp.2006.06.019

Morley, S. K., Friedel, R. H. W., Spanswick, E. L., Reeves, G. D., Steinberg, J. T., Koller, J., et al. (2010). Dropouts of the outer electron radiation belt in response to solar wind stream interfaces: Global Positioning System observations. *Proceedings of the Royal Society of London A: Mathematical, Physical and Engineering Sciences*, *466*(2123), 3329–3350. https://doi.org/10.1098/rspa.2010.0078

Morley, S. K., Henderson, M. G., Reeves, G. D., Friedel, R. H. W., & Baker, D. N. (2013). Phase space density matching of relativistic electrons using the Van Allen Probes: REPT results. *Geophysical Research Letters*, *40*, 4798–4802. https://doi.org/10.1002/grl.50909

Morley, S. K., Sullivan, J. P., Carver, M. R., Kippen, R. M., Friedel, R. H. W., Reeves, G. D., & Henderson, M. G. (2017). Energetic particle data from the Global Positioning System constellation. *Space Weather*, *15*, 283–289. https://doi.org/10.1002/2017SW001604

Morley, S. K., Sullivan, J. P., Henderson, M. G., Blake, J. B., & Baker, D. N. (2016). The Global Positioning System constellation as a space weather monitor: Comparison of electron measurements with Van Allen Probes data. *Space Weather*, *14*, 76–92. https://doi.org/10.1002/2015SW001339

Murphy, K. R., Mann, I. R., & Sibeck, D. G. (2015). On the dependence of storm time ULF wave power on magnetopause location: Impacts for ULF wave radial diffusion. *Geophysical Research Letters*, *42*, 9676–9684. https://doi.org/10.1002/2015GL066592

Omura, Y., Furuya, N., & Summers, D. (2007). Relativistic turning acceleration of resonant electrons by coherent whistler mode waves in a dipole magnetic field. *Journal of Geophysical Research*, *112*, A06236. https://doi.org/10.1029/2006JA012243

Ozeke, L. G., Mann, I. R., Murphy, K. R., Sibeck, D. G., & Baker, D. N. (2017). Ultra-relativistic radiation belt extinction and ULF wave radial diffusion: Modeling the September 2014 extended dropout event. *Geophysical Research Letters*, *44*, 2624–2633. https://doi.org/10.1002/2017GL072811

Roederer, J. (1970). *Dynamics of geomagnetically trapped radiation*, Physics and Chemistry in Space. New York: Springer-Verlag.

Schulz, M., & Lanzerotti, L. J. (1974). *Particle diffusion in the radiation belts*, Physics and Chemistry in Space. Berlin: Springer.

Shprits, Y. Y., Drozdov, A. Y., Spasojevic, M., Kellerman, A. C., Usanova, M. E., Engebretson, M. J., et al. (2016). Wave-induced loss of ultra-relativistic electrons in the Van Allen radiation belts. *Nature Communications*, *7*, 12883. https://doi.org/10.1038/ncomms12883

Shprits, Y. Y., Horne, R. B., Kellerman, A. C., & Drozdov, A. Y. (2018). The dynamics of Van Allen belts revisited. *Nature Physics*, *14*(2), 102–103. https://doi.org/10.1038/nphys4350

Shprits, Y. Y., Meredith, N. P., & Thorne, R. M. (2007). Parameterization of radiation belt electron loss timescales due to interactions with chorus waves. *Geophysical Research Letters*, *34*, L11110. https://doi.org/10.1029/2006GL029050

Shprits, Y. Y., Subbotin, D., Drozdov, A., Usanova, M. E., Kellerman, A., Orlova, K., et al. (2013). Unusual stable trapping of the ultrarelativistic electrons in the Van Allen radiation belts. *Nature Physics*, *9*(11), 699–703. https://doi.org/10.1038/nphys2760

Shprits, Y. Y., Subbotin, D. A., Meredith, N. P., & Elkington, S. R. (2008). Review of modeling of losses and sources of relativistic electrons in the outer radiation belt II: Local acceleration and loss. *Journal of Atmospheric and Solar-Terrestrial Physics*, *70*(14), 1694–1713. https://doi.org/10.1016/j.jastp.2008.06.014, dynamic Variability of Earth's Radiation Belts.

Shprits, Y. Y., Thorne, R. M., Friedel, R., Reeves, G. D., Fennell, J., Baker, D. N., & Kanekal, S. G. (2006). Outward radial diffusion driven by losses at magnetopause. *Journal of Geophysical Research*, *111*, A11214. https://doi.org/10.1029/2006JA011657

Shue, J.-H., Song, P., Russell, C. T., Steinberg, J. T., Chao, J. K., Zastenker, G., et al. (1998). Magnetopause location under extreme solar wind conditions. *Journal of Geophysical Research*, *103*(A8), 17,691–17,700. https://doi.org/10.1029/98JA01103

Spence, H. E., Reeves, G. D., Baker, D. N., Blake, J. B., Bolton, M., Bourdarie, S., et al. (2013). Science goals and overview of the Radiation Belt Storm Probes (RBSP) energetic particle, composition, and thermal plasma (ECT) suite on NASA's Van Allen Probes Mission. *Space Science Reviews*, *179*(1), 311–336. https://doi.org/10.1007/s11214-013-0007-5

Summers, D., & Thorne, R. M. (2003). Relativistic electron pitch-angle scattering by electromagnetic ion cyclotron waves during geomagnetic storms. *Journal of Geophysical Research*, *108*(A4), 1143. https://doi.org/10.1029/2002JA009489

Thorne, R. M., Li, W., Ni, B., Ma, Q., Bortnik, J., Chen, L., et al. (2013). Rapid local acceleration of relativistic radiation-belt electrons by magnetospheric chorus. *Nature*, *504*(7480), 411–414. https://doi.org/10.1038/nature12889

Thorne, R. M., Smith, E. J., Burton, R. K., & Holzer, R. E. (1973). Plasmaspheric hiss. *Journal of Geophysical Research*, *78*(10), 1581–1596. https://doi.org/10.1029/JA078i010p01581

Tsyganenko, N. A., & Sitnov, M. I. (2005). Modeling the dynamics of the inner magnetosphere during strong geomagnetic storms. *Journal of Geophysical Research*, *110*, A03208. https://doi.org/10.1029/2004JA010798

Turner, D. L., Shprits, Y., Hartinger, M., & Angelopoulos, V. (2012). Explaining sudden losses of outer radiation belt electrons during geomagnetic storms. *Nature Physics*, *8*, 208–212. https://doi.org/10.1038/nphys2185

Tuszewski, M., Cayton, T. E., Ingraham, J. C., & Kippen, R. M. (2004). Bremsstrahlung effects in energetic particle detectors. *Space Weather*, *2*, S10S01. https://doi.org/10.1029/2003SW000057

Ukhorskiy, A. Y., Sitnov, M. I., Millan, R. M., & Kress, B. T. (2011). The role of drift orbit bifurcations in energization and loss of electrons in the outer radiation belt. *Journal of Geophysical Research*, *116*, A09208. https://doi.org/10.1029/2011JA016623

Usanova, M. E., Drozdov, A., Orlova, K., Mann, I. R., Shprits, Y., Robertson, M. T., et al. (2014). Effect of EMIC waves on relativistic and ultrarelativistic electron populations: Ground-based and Van Allen Probes observations. *Geophysical Research Letters*, *41*, 1375–1381. https://doi.org/10.1002/2013GL059024

Van Allen, J. A., & Frank, L. A. (1959). Radiation around the Earth to a radial distance of 107,400 km. *Nature*, *183*, 430–434. https://doi.org/10.1038/183430a0

Wrenn, G. L. (1995). Conclusive evidence for internal dielectric charging anomalies on geosynchronous communications spacecraft. *Journal of Spacecraft and Rockets*, *32*(3), 514–520. https://doi.org/10.2514/3.26645

Xiang, Z., Tu, W., Li, X., Ni, B., Morley, S. K., & Baker, D. N. (2017). Understanding the mechanisms of radiation belt dropouts observed by Van Allen Probes. *Journal of Geophysical Research: Space Physics*, *122*, 9858–9879. https://doi.org/10.1002/2017JA024487

Yu, Y., Koller, J., Zaharia, S., & Jordanova, V. (2012). L* neural networks from different magnetic field models and their applicability. *Space Weather*, *10*, s02014. https://doi.org/10.1029/2011SW000743